Remote Sensing of Environment 154 (2014) 38–45

Contents lists available at ScienceDirect

Remote Sensing of Environment

journal homepage: www.elsevier.com/locate/rse

Mapping maximum urban air temperature on hot summer days

Hung Chak Ho [a,*], Anders Knudby [a], Paul Sirovyak [a], Yongming Xu [b], Matus Hodul [a], Sarah B. Henderson [c,d]

[a] Department of Geography, Simon Fraser University, Burnaby, BC, Canada
[b] School of Remote Sensing, Nanjing University of Information Science & Technology, Nanjing, China
[c] School of Population and Public Health, University of British Columbia, Vancouver, BC, Canada
[d] BC Centre for Disease Control, Vancouver, BC, Canada

ARTICLE INFO

Article history:
Received 4 April 2014
Received in revised form 4 July 2014
Accepted 6 August 2014
Available online xxxx

Keywords:
Landsat
Air temperature
Urban
Spatial modeling
Remote sensing application
Random forest
Statistical model
Urban heat island

ABSTRACT

Air temperature is an essential component in microclimate and environmental health research, but difficult to map in urban environments because of strong temperature gradients. We introduce a spatial regression approach to map the peak daytime air temperature relative to a reference station on typical hot summer days using Vancouver, Canada as a case study. Three regression models, ordinary least squares regression, support vector machine, and random forest, were all calibrated using Landsat TM/ETM+ data and field observations from two sources: Environment Canada and the Weather Underground. Results based on cross-validation indicate that the random forest model produced the lowest prediction errors (RMSE = 2.31 °C). Some weather stations were consistently cooler/hotter than the reference station and were predicted well, while other stations, particularly those close to the ocean, showed greater temperature variability and were predicted with greater errors. A few stations, most of which were from the Weather Underground data set, were very poorly predicted and possibly unrepresentative of air temperature in the area. The random forest model generally produced a sensible map of temperature distribution in the area. The spatial regression approach appears useful for mapping intra-urban air temperature variability and can easily be applied to other cities.

1. Introduction

Near-surface air temperature, defined as the temperature 2 m above the land surface, is a key variable in studies of meteorology, climate, and environmental health (Garske, Ferguson, & Ghani, 2013; Harvell et al., 2002; Katsouyanni et al., 1993; Koken et al., 2003; Kuhn, Campbell-Lendrum, & Davies, 2002; Maria & Renganathan, 2008; Nichol, Fung, Lam, & Wong, 2009; Oke & Maxwell, 1975; Saaroni & Baruch, 2010). Previous studies have widely used air temperature to estimate the intensity of urban heat islands (Kolokotroni & Giridharan, 2008; Unger, Sümeghya, & Zobokib, 2001), to study the relationship air temperature and air pollution (Koken et al., 2003), and to predict risks of heat-related mortality (Laaidi et al., 2012). Air temperature is traditionally monitored by stationary meteorological instruments (weather stations), which provide point data with high temporal frequency, typically recorded on an hourly basis. However, such observations are often unable to adequately describe spatial heterogeneity over small geographic extents (Benali, Carvalho, Nunes, Carvalhais, & Santos, 2012). This is particularly important in thermally complex environments such as urban settings, where local microclimatic variability is influenced by factors such as land cover (Saaroni & Baruch, 2010), exposure to wind and sun, soil and vegetation moisture, and the thermal properties of upwind areas (Oke & Maxwell, 1975). Spatial patterns in these variables exist at very fine scales (10^1–10^2 m) compared with the sampling density typically provided by weather station networks (10^4–10^5 m), suggesting that spatial interpolation between station observations is not an optimal solution for mapping air temperature in the urban environment (Vogt, Viau, & Paquet, 1997). Remote sensing provides an additional source of data that can provide high-resolution spatially explicit information on many of the factors that influence air temperature and thus assist with mapping it in spatially heterogeneous environments. Three principal approaches have been used to map air temperature from remote sensing data: 1) the Temperature–Vegetation Index (TVX), 2) energy balance models, and 3) statistical analyses (Benali et al., 2012; Zakšek & Schroedter-Homscheidt, 2009).

The TVX method is based on the hypothesis that while an unvegetated surface can be substantially warmer than the surrounding air, the surface temperature of an infinitely thick vegetation canopy will approximate the air temperature because the canopy consists primarily of air, with branches and leaves volumetrically a minor component. On that basis, Prihodko and Goward (1997) used the observed negative correlation between the Normalized Difference Vegetation Index (NDVI) and Land Surface Temperature (LST), as well as an estimate of the NDVI value for an infinitely thick canopy, to estimate air temperature. To employ the TVX method, a sample window with varying vegetation cover is needed for the establishment of local NDVI–LST correlations. In addition to requiring local variations in vegetation cover, the use of a sample

* Corresponding author.
E-mail address: hohungh@sfu.ca (H.C. Ho).

http://dx.doi.org/10.1016/j.rse.2014.08.012
0034-4257/

window effectively reduces the spatial resolution of the predicted air temperatures and makes the TVX method best suited for large regions with gradual temperature changes (e.g. Sandholt, Rasmussen, & Andersen, 2002; Stisen, Sandholt, Norgaard, Fensholt, & Eklundh, 2007; Vancutsem, Ceccato, Dinku, & Connor, 2010; Zhu, Lu, & Jia, 2013) but unsuitable for urban areas.

The energy balance approach considers air temperature to be controlled by Earth system energy dynamics, including the radiation balance as well as soil, sensible, and latent heat fluxes (Meteotest, 2010; Oke, 1988; Sun et al., 2005). It is thus directly grounded in thermodynamics, but it relies on comprehensive parameterization for which spatially distributed data are rarely available, specifically at the resolution necessary for application to urban studies (Mostovoy, King, Reddy, Kakani, & Filippova, 2006).

Statistical analyses are mostly based on empirical regression modeling, which can take the form of linear (Nichol et al., 2009) or more complex statistical models like neural networks, genetic algorithms and regression trees (Emamifar, Rahimikhoob, & Noroozi, 2013; Jang, Viau, & Anctil, 2004; Singh, Joshi, & Kishtawal, 2006). Predictors of air temperature can be limited to land surface temperature (LST) (Mostovoy et al., 2006), or also include one or more additional environmental variables (Benali et al., 2012) such as NDVI, elevation, and land cover. Regression models can be suitable for areas with complex landscape characteristics, such as urban areas, although application will generally be limited to the environment for which they were developed.

Remote sensing-based air temperature mapping has typically focused on relatively large (>100,000 km^2) and homogeneous geographic regions (Benali et al., 2012; Mostovoy et al., 2006; Stisen et al., 2007; Vogt et al., 1997; Xu, Qin, & Shen, 2012). Few existing studies have attempted to map air temperature distributions at the city scale; the only notable example is provided by Nichol and To (2012) studying the distribution of air temperature in Kowloon, Hong Kong. The development and validation of approaches optimized to map air temperature distributions in urban environments is of particular importance in the context of extreme heat events and their impacts on human health, which are expected to increase in severity in the future. Specifically, development of a method to map peak daytime air temperature (Tmax) is of importance because this variable is commonly used to quantify the relationship between extreme heat and mortality (Kunst, Looman, & Mackenback, 1993; Medina-Ramon, Zanobetti, Cavanagh, & Schwartz, 2006), and recent studies indicate that maps of temperature during extreme heat events can help explain the spatial pattern of heat-related risk (Anderson & Bell, 2011; Buscail, Upegui, & Viel, 2012; Hondula et al., 2012; Laaidi et al., 2012; Tomlinson, Chapman, Thornes, & Baker, 2011). However, to be useful for heat emergency planning purposes, Tmax maps must be valid for typical (as opposed to specific) hot summer days, which precludes mapping of absolute temperature values that vary depending on the severity of the heat wave.

In this study, we assess the ability of three remote sensing-based regression models to map Tmax for the Greater Vancouver region of British Columbia, Canada, using Landsat data and point observations from weather stations in the area. The methods are ordinary least squares regression, support vector machine, and random forest. We quantify Tmax relative to Vancouver International Airport (YVR), as forecasted and observed temperatures at this weather station form the basis for heat health emergency definitions for the area.

2 . Study Area

Our study area is Greater Vancouver, British Columbia, Canada (Fig. 1), a coastal metropolitan area with >2 million people (Statistics Canada, 2007). Greater Vancouver is bordered to the north by fold mountain ridges, to the west by the Pacific Ocean, and to the east by the semi-arid Fraser Valley, a geographic context that generates a complex microclimate in the area (Oke, 1976; Oke & Hay, 1994; Runnalls & Oke, 2000). During the summer, ocean breezes and winds from the mountain ridges can cool down the coastal regions, while the Fraser Valley can trap air masses and create a relatively hot zone (Oke & Hay, 1994). Temperature in the urban area is heavily influenced by cloud cover in the summer period, while evaporative cooling is of little influence due to limited vegetation cover. On a hot summer day Greater Vancouver is typically cloudless with light winds from the Fraser Valley, a weather situation that can generate a strong urban heat island effect and substantially higher temperatures in the urban areas compared with their surroundings (Oke & Hay, 1994).

3 . Data and methods

3.1 . Satellite data

The satellite data used in this study consist of all (n = 6) cloud-free Landsat 5 TM and Landsat 7 ETM+ images available from 2001 to 2010 for hot summer days in the study area, here defined as days with Tmax > 25 °C at YVR (Table 1). 25 m Canadian Digital Elevation Data (CDED, http://www.geobase.ca) were used to provide elevation information for the study area. Landsat 5 TM images and the DEM were resampled to 60 m to match the spatial resolution of the ETM+ thermal band, and all data were projected to UTM zone 10 N.

3.2 . Satellite-derived predictors

Several spatial data layers were derived from the Landsat and elevation data for use as predictors in regression models to map Tmax: LST, Normalized Difference Water Index (NDWI), elevation, skyview factor (SVF), and solar radiation. All layers except elevation were derived separately for each Landsat image.

LST was estimated from Landsat band 6. Top of atmosphere radiance values were atmospherically corrected using NASA's Atmospheric Correction Parameter Calculator to obtain at-surface radiance (Barsi, Barker, & Schott, 2003), and kinetic surface temperature was then derived by inversion of Planck's Law, applying emissivity values from the North American ASTER Land Surface Emissivity Database (Hulley & Hook, 2009).

$$LST = K_2 / \ln(\varepsilon K_1 L_\lambda + 1)$$

where K_1 and K_2 are the coefficients, ε is the emissivity and L_λ is the radiance.

NDWI is an index designed to quantify vegetation water content (Gao, 1996), which strongly influences surface cooling through evapotranspiration. NDWI is defined as:

$$NDWI = (\rho_{NIR} - \rho_{MIR})/(\rho_{NIR} + \rho_{MIR})$$

In this study, Landsat bands 4 and 5 were used to calculate NDWI for land areas. NDWI values are not meaningful over water and, as both ρ_{NIR} and ρ_{MIR} are very small over water, tend to be noisy. To allow the NDWI layer to function as a proxy for cooling by evapotranspiration, we found the maximum NDWI value on land and applied it to all water surfaces, replacing the results from the original NDWI calculation for water.

SVF can be defined as the portion of unobscured sky, which is related to the radiation received or emitted in an area (Chen et al., 2012; Su, Brauer, & Buzzelli, 2008) and is influenced by both topography and building structure. SVF was mapped for each pixel using an empirically calibrated relationship with shadow proportion, which was derived using partial spectral unmixing. Full details of the method used to derive the SVF data layer will be forthcoming in a separate paper; validation using independent lidar data for Vancouver shows the method to perform well (SVF root mean square error = 0.056).

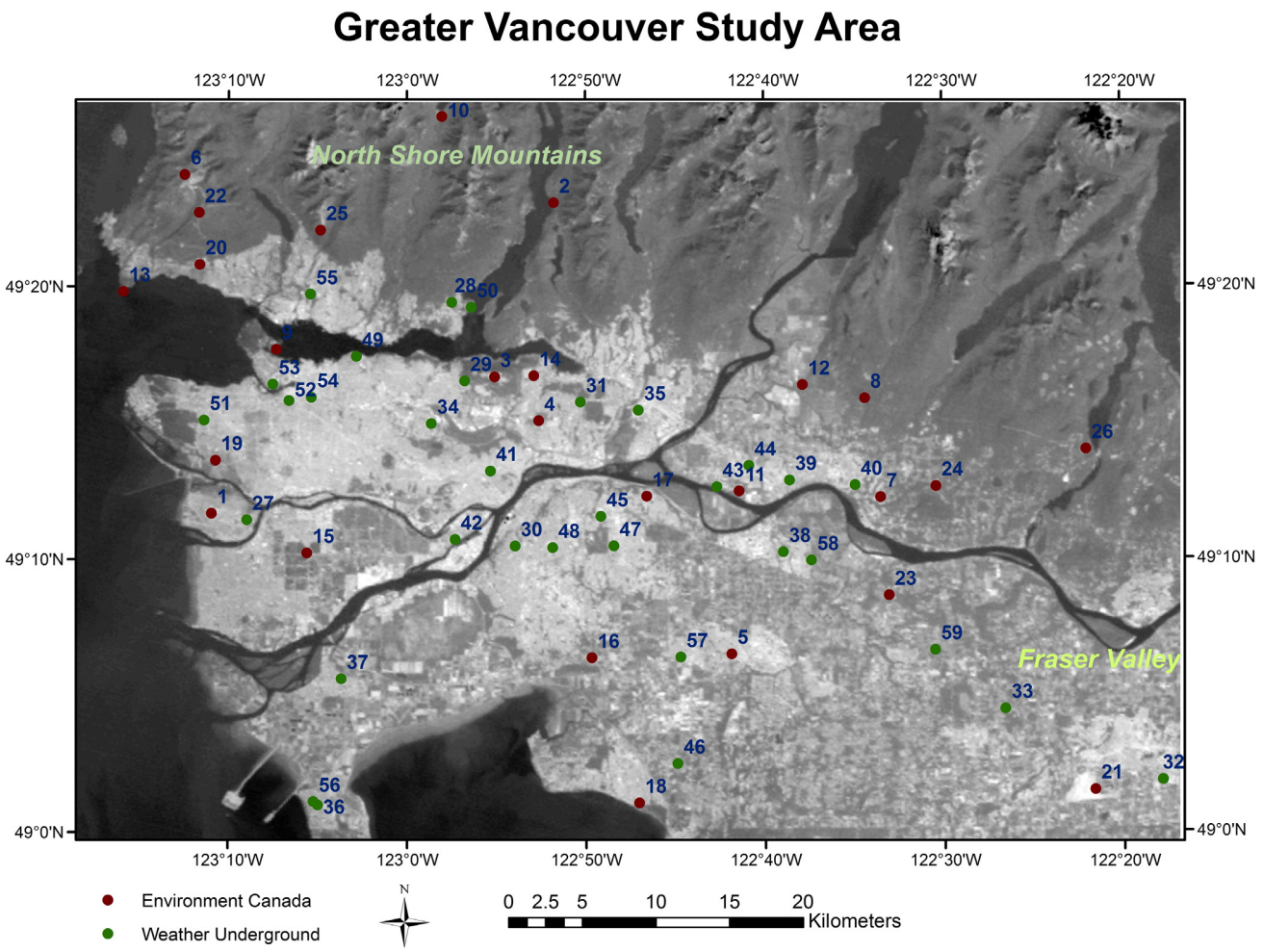

Fig. 1. Study area and the location of weather stations operated by Environment Canada (red) and the Weather Underground (green). (For interpretation of the references to color in this figure legend, the reader is referred to the web version of this article.)

Incoming solar radiation has also been shown to influence air temperature (Bristow & Campbell, 1984). Incoming solar radiation was estimated using an implementation of the direct solar radiation equation (Fu & Rich, 2002) in ArcGIS 10.1, which assumes that the total direct solar radiation is the sum of direct solar radiation from all sun map sectors. It is defined as:

$$\text{Solar Radiation} = S_{Const}\beta^{m(\theta)} \times \text{SunDur}_{\theta,\alpha} \times \text{SunGap}_{\theta,\alpha} \times \cos\left(\text{AngIn}_{\theta,\alpha}\right)$$

where S_{Const} = solar flux, β = atmospheric transmittance, $m(\theta)$ = optical path length, $\text{SunDur}_{\theta,\alpha}$ = time duration represented by sky sector, $\text{SunGap}_{\theta,\alpha}$ = gap fraction for the sun map sector, $\text{AngIn}_{\theta,\alpha}$ = incident angle, and θ = solar zenith angle.

Several additional factors known to correlate with local air temperature were not included in our model. Preliminary analyses showed that NDVI, which is designed to quantify photosynthetic activity, did not increase the predictive power of models that already included NDWI, which is designed to quantify vegetation water content and thus is more directly related to evapotranspiration and air temperature. A similar result was found by Benali et al. (2012). Land cover information was not directly incorporated in the model, but is indirectly quantified by LST and NDWI, which are both strongly influenced by land cover, and SVF, which is determined by three-dimensional surface structure and thus also influenced by land cover. Wind speed and direction, despite being known to strongly influence local air temperature, were not included because of their temporal variability as well as a lack of wind data with sufficient spatial resolution.

Table 1
Landsat images used in this study. The images were obtained for cloud-free hot summer days in Greater Vancouver.

Satellite images	Acquired date	Daily maximum air temperature at Vancouver International Airport
Landsat 5 TM	13/08/2002	27.1
Landsat 5 TM	17/07/2004	27.1
Landsat 7 ETM +	02/08/2004	25.4
Landsat 5 TM	23/07/2006	26.7
Landsat 5 TM	12/07/2008	25.5
Landsat 7 ETM +	31/07/2009	28.7

3.3 . Calibration/validation data

In addition to the spatial data layers, Tmax observations from 59 weather stations in the study area were used for calibration and validation of the regression models for mapping air temperature (Fig. 1). 26 of the weather stations are operated by Environment Canada (EC), and the other 33 stations are included in the Weather Underground (WU) network, a public participation weather project in which individuals can deploy personal weather stations and have the resulting data

uploaded to a publicly accessible geodatabase (Goodchild, 2007; Sieber, 2006). Not all weather stations were operational for all of the six days used in our study, including several of the WU stations for which data were only available for one or two of the latest dates.

3.4 . Regression models

Regression models, using predictors derived from satellite and elevation data, were first used to predict the absolute Tmax observed at weather stations for each of the six days for which Landsat data were available, and Tmax values were then normalized relative to the corresponding Tmax value at YVR. Ultimately the six maps of relative Tmax were averaged to describe Tmax, relative to YVR, for a typical hot summer day in the study area. Per-pixel predictions of absolute temperature were based on the pixel values of elevation, SVF and solar radiation, as well as spatially averaged values of LST and NDWI, calculated for circular areas with radii of 100, 200, 400, 600, 800, and 1000 m surrounding each pixel. The spatial averaging was used to account for the influence of temperature and moisture surface conditions in the areas surrounding each station (Liu & Moore, 1998; Zakšek & Oštir, 2012), and the specific radii were selected to cover the range from the smallest meaningful radius, given the 60 m spatial resolution of the data, to the largest radius within which the predictors were expected to influence Tmax. Additional research on the spatial dependence of interaction between surface properties and air temperature could inform better selection of these radii in future studies.

Three types of statistical models were used to predict Tmax from the 15 predictors: 1) Ordinary least squares multiple linear regression, 2) support vector machine (SVM), and 3) random forest. Ordinary least squares regression uses the observed data to estimate the parameters of a linear regression function (Kutner, Nachtsheim, & Neter, 2004). SVM is a machine learning based regression model initially developed for classification problems. It determines the location of decision boundaries and uses the boundaries to predict optimal separation of classes (Cortes & Vapnik, 1995; Mountrakis, Im, & Ogole, 2011; Pal & Mather, 2005). Previous remote sensing studies have primarily used this method for classification (Huang, Davis, & Townshend, 2002; Melgani & Bruzzone, 2004; Ocak & Seker, 2013; Oommen et al., 2008; Pal & Mather, 2005) but Bruzzone and Melgani (2005) developed an SVM-based conceptual multiple estimator system for biophysical parameter prediction. This system successfully develops a regression-based SVM and is widely applied to predict continuous output in environmental studies (Camps-Valls, Bruzzone, Rojo-Alvarez, & Melgani, 2006; Camps-Valls et al., 2006; Das, Samui, Sabat, & Sitharam, 2010; Durbha, King, & Younan, 2007; Knudby, Brenning, & LeDrew, 2010; Knudby, LeDrew, & Brenning, 2010; Mountrakis et al., 2011; Sun, Li, & Wang, 2009). Random forest is a nonlinear ensemble machine learning model using multiple regression trees, where each tree is trained on a random subset of the training data and each split in each tree is determined using a random subsample of the available predictors (Breiman, 2001; Stumpf & Kerle, 2011; Timm & McGraigal, 2012). R and its contributed packages (raster, e1071, and randomForest) were used to develop and apply the statistical models using default model parameter settings (Hijmans & van Etten, 2009; Liaw & Wiener, 2012; Meyer, Dimitriadou, Hornik, Weingessel, & Leisch, 2012; R Core Development Team, 2008).

3.5 . Accuracy assessment

To quantify the prediction error expected for an unsampled area, each regression model was calibrated using observations from all weather stations except one, and predictions for that station were then compared to the observations to determine prediction error. This leave-one-out process was repeated using observations from each station for validation once. Using all data from a given weather station in either the calibration or validation data set ensured that this cross-validation procedure provided a good estimate of typical prediction errors for an unsampled location. Cross-validation is a widely recognized error assessment method frequently used to validate machine learning models such as random forest and SVM (Gislason, Benediktsson, & Sveinsson, 2006). The mean absolute error (MAE) and root mean square error (RMSE) were used to quantify errors (Willmott & Matsuura, 2005), and the model with the lowest error values was ultimately used to create a relative Tmax map for Greater Vancouver.

3.6 . Variance importance analysis

A model-independent permutation-based analysis was used to assess the influence of the individual predictors in the most accurate model (Genuer, Poggi, & Tuleau-Malot, 2010; Knudby, LeDrew, et al., 2010; Strobl, Malley, & Tutz, 2009). During this analysis, a model was calibrated using a subset (63.2%) of all observations and validated by quantifying the prediction error for the remaining observations. The values of one predictor were then randomly permuted in the validation data, new predictions produced, and the percentage increase in mean squared error (%IncMSE) caused by the permutation was calculated. This permutation was repeated for each predictor to quantify the relative increase in prediction error caused by permutation of the individual predictors.

4 . Results

4.1 . Model performance

The MAE and RMSE values were similar for all models (Table 2), ranging from 1.82 to 1.93 °C and from 2.31 to 2.46 °C respectively, which is comparable with previous remote sensing-based air temperature mapping studies (Benali et al., 2012; Czajkowski, Goward, Stadler, & Walz, 2000; Prihodko & Goward, 1997; Vancutsem et al., 2010; Zakšek & Schroedter-Homscheidt, 2009; Zhu et al., 2013). The random forest model outperformed the other model types slightly, and was therefore retained for further analysis and mapping.

Observations with very high Tmax values were consistently underestimated by the model, and observations with very low Tmax values were consistently underestimated (Fig. 2). This is partly an inevitable result of the model specification, where the air temperature predictions for a typical hot summer day are compared with observations for all hot summer days, some typical and some extreme. It may also result from the fact that several environmental variables with known influence on air temperature were not included as predictors in the model, such as wind speed and direction, turbulence, and anthropogenic heat, all of which may influence air temperature at very small spatial scales.

4.2 . Spatial distribution of relative maximum air temperature

The map of Tmax distribution in the study area (Fig. 3) was produced by application of the random forest model to each of the four Landsat 5 images and calculation of the average per-pixel Tmax prediction from each image. The two Landsat 7 images were excluded from this map production as their Scan-Line Corrector errors produced substantial local artifacts. The map presents a sensible description of the spatial distribution of air temperature in the study area. Low

Table 2
Maximum air temperature (Tmax) error estimates based on cross-validation, for each model type.

Model	MAE	RMSE
Random forest	1.82 °C	2.31 °C
Support vector machine	1.91 °C	2.46 °C
Ordinary least squares regression	1.93 °C	2.46 °C

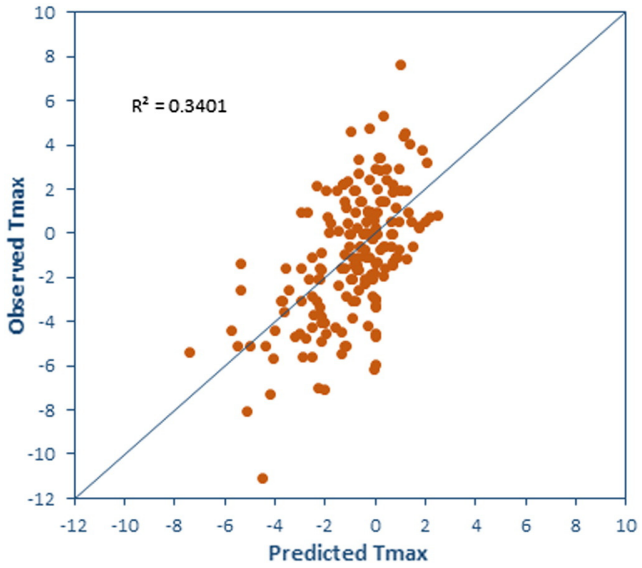

Fig. 2. Scatter plot of the observed versus predicted relative maximum air temperature (Tmax) using the random forest model.

temperatures are predicted in the mountainous area north of Vancouver, particularly at high elevations, while high temperatures are predicted in the urban/suburban residential areas. Agricultural areas are predicted to be relatively cool, and forests are consistently predicted to be cool. These predictions correspond well with past studies of air temperature distribution in the area (Oke & Hay, 1994; Prihodko & Goward, 1997; Weng, Lu, & Schubring, 2004). Downtown Vancouver is predicted to be relatively cool compared with other parts of the metropolitan area. This can be the result of the proximity of downtown to the ocean, which is known to be an important controlling factor of Tmax in Vancouver (Runnalls & Oke, 2000), especially when winds from the ocean cool down the coastal areas. Downtown also has low SVF values due to the high density of tall buildings. This reduces direct solar insolation and thus dampens the daily temperature cycle leading to lower Tmax. In addition, the tall buildings may also create an urban canyon with a "wall effect" (Wong, Nichol, & Ng, 2011) that controls the wind direction in the urban area and reduces airflow by trapping air masses within the downtown area. This isolating effect may create a relatively cold zone in the area dominated by high-rise buildings, where the cool air from the early morning and previous night is only slowly heated. Unfortunately, no field observations were available from downtown Vancouver for this study; future data collection will be used to update and validate the model predictions for this area.

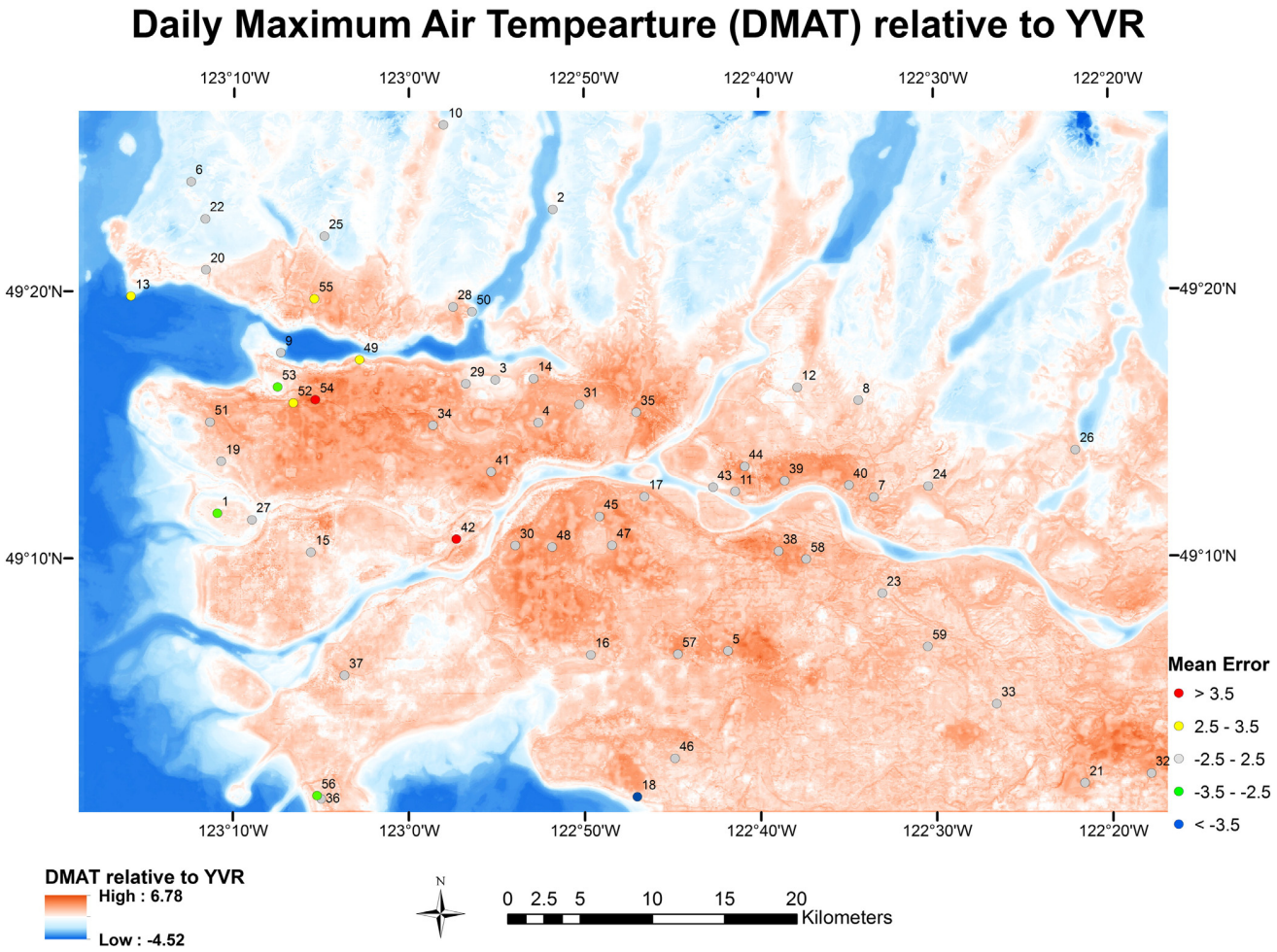

Fig. 3. Map showing the average distribution of daily maximum air temperature (Tmax) relative to Vancouver International Airport, produced with the Random forest model. Points indicate all weather stations used for calibration/validation. Point color indicates mean error values for each station. (For interpretation of the references to color in this figure legend, the reader is referred to the web version of this article.)

Table 3
Results from variable important analyses. The percentage increase in mean squared error (%IncMSE) quantifies the increase in prediction error caused by permutation of each individual predictor.

Variable	%IncMSE
LST (1000 m)	17.489371
LST (600 m)	15.932648
Solar	15.874094
LST (800 m)	14.846949
LST (100 m)	14.702946
LST (400 m)	13.237163
SVF	13.174871
NDWI (200 m)	12.744121
NDWI (600 m)	12.712283
LST (200 m)	12.580855
NDWI (400 m)	12.296493
NDWI (100 m)	11.654815
NDWI (800 m)	11.422394
NDWI (1000 m)	9.388323
Elevation	7.436711

4.3. Variable importance

All LST variables had high importance scores, as did solar radiation (Table 3). Positive importance scores for every variable are an indication that all variables have contributed to the model predictions. LST and solar radiation have previously been found to play a strong role in determining maximum air temperature for a typical hot summer day (Bristow & Campbell, 1984; Vancutsem et al., 2010), and receive the highest variable importance scores in our model. LST calculated at the largest radius (1000 m) had the highest score of any predictor, emphasizing the effect of LST in neighboring areas on air temperature. The influence of NDWI could show the cooling effect of evapotranspiration in areas with relatively wetter vegetation and/or the shading effect of vegetation. The importance of SVF is fair, and is more than half of the most important variable. Given the concentration of low SVF areas around downtown Vancouver, where no weather stations are located, the actual influence of SVF on air temperature is likely to be underestimated by the variable importance results. A similar effect is likely the cause of elevation having the lowest variable importance, as only a few weather stations are located at elevations above 100 m. The permutation of both the SVF and elevation variables will therefore cause only a negligible change in the validation data.

In addition, we note that it is difficult to assess the importance of any individual variable in a multivariate model, as the calculated importance of each variable is influenced by the presence of other correlated or interacting variables in a dataset, i.e. multicollinearity (Murray & Conner, 2009). Model structure can also affect variable importance, for example predictors related non-linearly to the response will have higher importance in nonlinear than linear models (Knudby, LeDrew, et al., 2010). More fundamentally, predictors that have themselves been mapped with low accuracy will, all other things being equal, have relatively low variable importance. Variable importance results, including ours, should thus only be interpreted with caution and in the light of other available evidence.

5 . Discussion

5.1. Temperature pattern variability

An implicit assumption behind mapping the distribution of Tmax relative to YVR for a typical hot summer day is that such a typical distribution exists, in other words that relative Tmax is reasonably stable for hot summer days in the area and that the notion of typical Tmax is meaningful. There was in fact considerable variability of Tmax relative to YVR (Fig. 4). While some weather stations always recorded much higher temperatures than YVR (e.g. station 43) and some typically recorded lower temperatures (e.g. station 18), others (e.g. stations 4 and 20) show substantial variation in their temperatures relative to YVR. Further research should focus on identifying weather patterns or other factors that may control these variations.

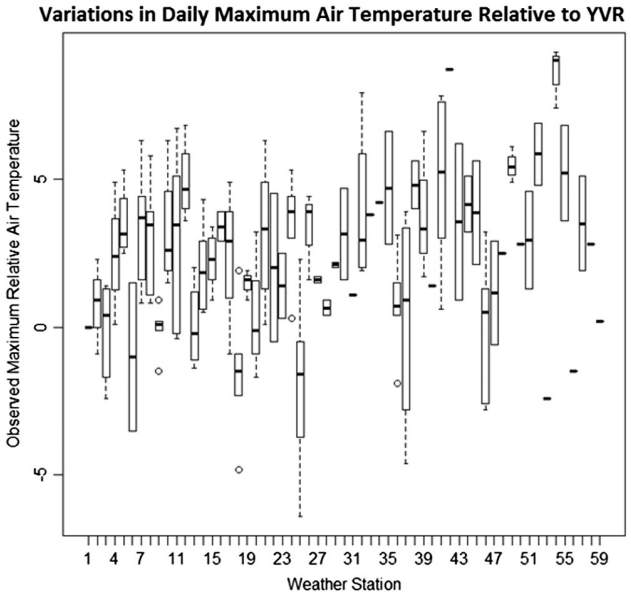

Fig. 4. Boxplot of variation in maximum daily air temperature (Tmax) relative to Vancouver International Airport (YVR).

To further investigate this issue, mean prediction errors (ME) for each station were calculated and used to separate stations into five groups: severely underestimated (ME > +3.5 °C); underestimated (+3.5 °C > ME > +2.5 °C); unbiased (+2.5 °C > ME > −2.5 °C); overestimated (−2.5 °C > ME > −3.5 °C); and severely overestimated (−3.5 °C > ME). A plot of these values on the map (Fig. 3) suggests that stations close to the ocean are predicted more poorly than those further inland, as nine of the 21 weather stations located within 5 km of the ocean are either overestimated or underestimated, compared with one of the 38 stations located further inland. It is likely that variable wind patterns are responsible for the poorer prediction in areas near the ocean, as the air temperature here is strongly influenced by sea breezes bringing cold ocean air eastward, and land breezes bringing hot air westward from the Fraser Valley (Runnalls & Oke, 2000). In comparison, areas further inland are likely to be less influenced by wind direction. The lack of high spatial resolution data on wind speed and direction may thus be an important limitation for mapping of typical air temperature patterns in urban environments. EC weather stations are intended to monitor regional weather patterns, and are by design located outside densely populated areas. In the absence of appropriate data, modeling of local winds may be possible using simulation software (e.g. WindNinja, WindWizard) and high-resolution digital surface models. To our knowledge the accuracy of wind simulations for urban environments is unknown, as is their potential utility for air temperature mapping.

5.2. Weather underground data

Although WU provides guidelines for deploying weather stations, data quality is not controlled and was not accounted for in this study. Potential problems with the WU data are also illustrated in the mean error map (Fig. 3), where it can be seen that air temperature is severely underestimated (ME > 2.5 °C) at six weather stations, of which five are from WU and only one is from EC. In other words, temperatures from 4% of EC weather stations and 15% of WU weather stations are severely

underestimated. This problem is less acute with respect to overestimation of air temperature, which is seen for two EC and two WU weather stations. Greater prediction errors for WU weather stations could be a result of improper placement of some WU weather stations (e.g. next to heat sources or close to a highly reflective surface). The use of WU data in addition to EC data for model calibration has both advantages and disadvantages. In our study area inclusion of WU data almost doubled the number of weather station locations for which data were available. In addition, the use of WU data complemented the spatial distribution of data from EC weather stations, as the former were primarily available from urbanized areas while the latter are deliberately located away from large buildings and other reflecting surfaces typical of the urban environment (World Meteorological Organization, 1996). However, the lack of quality control is likely to result in some stations being improperly placed or operated, introducing bias for model calibration. This issue will be of increasing importance in the future, as WU and other volunteered geographic information (VGI) projects produce increasing volumes of data with uncertain quality. One alternative to VGI for increasing the amount of calibration/validation data could be dedicated mobile temperature monitoring (Anderson et al., 2012), which lends itself better to quality control but requires additional resources.

5.3. Complementary data sources

Finally, to incorporate spatial information on diurnal temperature variations, integration of MODIS-derived predictors may be feasible. The higher temporal resolution of MODIS images, and especially the early afternoon overpass of the Aqua satellite, may allow a description of energy balance dynamics that is better resolved in time and closer to the typical time of peak temperature (between 3 and 5 pm in our study area). The use of VGI, wind simulation software, and MODIS data may all be avenues to improve the modeling of air temperature in urban environments and achieve lower error values than those reported here.

6 . Conclusion

Few studies have attempted to map temperature distributions in urban areas using remote sensing. We demonstrated the ability of a regression model, calibrated with multiple Landsat scenes and weather station data for hot summer days, to produce a sensible map of daily maximum air temperature distribution in Greater Vancouver. Prediction errors (RMSE = 2.31 °C) are comparable with those reported in previous studies, despite the complex landscape of the area. In addition, the mapped predictions of Tmax relative to a reference station (YVR) correspond well with previous descriptions of air temperature distribution in the area, and are explained well by local differences in land cover, surface temperature, elevation, and distance to the ocean. Specifically for downtown Vancouver, the low skyview factor and proximity to the ocean results in relatively low Tmax values compared with the surrounding suburban areas. The ability to map the spatial distribution of Tmax in a large metropolitan area contributes a spatial dimension to urban heat studies, which in the past have relied on a single reference station to approximate air temperature for large and often heterogeneous areas.

Acknowledgment

The authors acknowledge the Pacific Institute for Climate Solutions and Simon Fraser University for partial funding of this project. We also thank Kaylee Girard, Spencer Behn and Melvin Pan for data processing, and three anonymous reviewers for constructive comments.

References

Anderson, G., & Bell, M. (2011). Heat waves in the United States: Mortality risk during heat waves and effect modification by heat wave characteristics in 43 U.S. communities. *Environmental Health Perspectives*, *119*(2), 210–218.
Anderson, A., Chapman, M., Drobot, S., Tadesse, A., Lambi, B., & Wiener, G. (2012). Quality of mobile air temperature and atmospheric pressure observations from the 2010 development test environment experiment. *Journal of Applied Meteorology and Climatology*, *51*(4), 691–701.
Barsi, J. A., Barker, J. L., & Schott, J. R. (2003). An Atmospheric Correction Parameter Calculator for a single thermal band earth-sensing instrument. *Toulouse, France: IGARSS IEEE International Geoscience and Remote Sensing Symposium*.
Benali, A., Carvalho, A., Nunes, J., Carvalhais, N., & Santos, A. (2012). Estimating air surface temperature in Portugal using MODIS LST data. *Remote Sensing of Environment*, *124*(2012), 108–121.
Breiman, L. (2001). Random forests. *Machine Learning*, *45*(1), 5–32.
Bristow, K., & Campbell, G. (1984). On the relationship between incoming solar radiation and daily maximum and minimum temperature. *Agricultural and Forest Meteorology*, *31*, 159–166.
Bruzzone, L., & Melgani, F. (2005). Robust multiple estimator systems for the analysis of biophysical parameters from remotely sensed data. *IEEE Transactions on Geoscience and Remote Sensing*, *43*(1), 159–174.
Buscail, C., Upegui, E., & Viel, J. -F. (2012). Mapping heatwave health risk at the community level for public health action. *International Journal of Health Geographics*, *11*, 38.
Camps-Valls, G., Bruzzone, L., Rojo-Alvarez, J. L., & Melgani, F. (2006). Robust support vector regression for biophysical variable estimation from remotely sensed images. *IEEE Geoscience and Remote Sensing Letters*, *3*(3), 339–343.
Camps-Valls, G., Gómez-Chova, L., Muñoz-Marí, J., Vila-Francés, J., Amorós-López, J., & Calpe-Maravilla, J. (2006). Retrieval of oceanic chlorophyll concentration with relevance vector machines. *Remote Sensing of Environment*, *105*(1), 23–33.
Chen, L., Ng, E., An, X., Ren, C., Lee, M., Wang, U., et al. (2012). Sky view factor analysis of street canyons and its implications for daytime intra-urban air temperature differentials in high-rise, high-density urban areas of Hong Kong: A GIS-based simulation approach. *International Journal of Climatology*, *32*, 121–136.
Cortes, C., & Vapnik, V. (1995). Support-vector networks. *Machine Learning*, *20*(3), 273–297.
Czajkowski, K. P., Goward, S. N., Stadler, S., & Walz, A. (2000). Thermal remote sensing of near surface environmental variables: Application over the Oklahoma Mesonet. *The Professional Geographer*, *52*(2), 345–357.
Das, S., Samui, P., Sabat, A., & Sitharam, T. (2010). Prediction of swelling pressure of soil using artificial intelligence techniques. *Environmental Earth Sciences*, *61*, 393–403.
Durbha, S., King, R., & Younan, N. (2007). Support vector machines regression for retrieval of leaf area index from multiangle imaging spectroradiometer. *Remote Sensing of Environment*, *107*(1–2), 348–361.
Emamifar, S., Rahimikhoob, A., & Noroozi, A. (2013). Daily mean temperature estimation from MODIS land surface temperature. *International Journal of Climatology*, http://dx.doi.org/10.1002/joc.3655.
Fu, P., & Rich, P. (2002). A geometric solar radiation model with applications in agriculture and forestry. *Computers and Electronics in Agriculture*, *37*, 25–35.
Gao, B. -C. (1996). NDWI—a normalized difference water index for remote sensing of vegetation liquid water from space. *Remote Sensing of Environment*, *58*, 257–266.
Garske, T., Ferguson, N., & Ghani, A. (2013). Estimating air temperature and its influence on malaria transmission across Africa. *PLoS One*, *8*(2), e56487.
Genuer, R., Poggi, J. -M., & Tuleau-Malot, C. (2010). Variable selection using random forests. *Pattern Recognition Letters*, *31*(14), 2225–2236.
Gislason, P., Benediktsson, J., & Sveinsson, J. (2006). Random forests for land cover classification. *Pattern Recognition Letters*, *27*, 294–300.
Goodchild, M. F. (2007). Citizens as sensors: The world of volunteered geography. *GeoJournal*, *69*(4), 211–221.
Harvell, C., Mitchell, C., Ward, J., Altizer, S., Dobson, A., Ostfeld, R., et al. (2002). Climate warming and disease risks for terrestrial and marine biota. *Science*, *296*(5576), 2158–2162.
Hijmans, R. J., & van Etten, J. (2009). Raster. Geographic analysis and modeling with raster data: R package version 0.9.8–40/r681. See. http://www.R-Forge.R-project.org/projects/raster/.fic (essay, and, social science essay)
Hondula, D., Davis, R., Leisten, M., Saha, M., Veazey, L., & Wegner, C. (2012). Fine-scale spatial variability of heat-related mortality in Philadelphia County, USA, from 1983–2008: A case-series analysis. *Environmental Health*, *11*, 16.
Huang, C., Davis, L., & Townshend, J. (2002). An assessment of support vector machines for land cover classification. *International Journal of Remote Sensing*, *23*(4), 725–749.
Hulley, G. C., & Hook, S. J. (2009). The North American ASTER Land Surface Emissivity Database (NAALSED) version 2.0. *Remote Sensing of Environment*, *113*(9), 1967–1975.
Jang, J., Viau, A., & Anctil, F. (2004). Neural network estimation of air temperatures from AVHRR data. *International Journal of Remote Sensing*, *25*(21), 4541–4554.
Katsouyanni, K., Pantazopoulou, A., Touloumi, G., Tselepidaki, I., Moustris, K., Asimakopoulos, D., et al. (1993). Evidence for interaction between air pollution and high temperature in the causation of excess mortality. *Archives of Environmental Health: An International Journal*, *48*(4), 235–242.
Knudby, A., Brenning, A., & LeDrew, E. (2010). New approaches to modelling fish-habitat relationships. *Ecological Modelling*, *221*, 503–511.
Knudby, A., LeDrew, E., & Brenning, A. (2010). Predictive mapping of reef fish species richness, diversity and biomass in Zanzibar using IKONOS imagery and machine-learning techniques. *Remote Sensing of Environment*, *114*(6), 1230–1241.
Koken, P., Piver, W., Ye, F., Elixhauser, A., Olsen, L., & Portier, C. (2003). Temperature, air pollution, and hospitalization for cardiovascular diseases among elderly people in Denver. *Environmental Health Perspectives*, *111*(10), 1312–1317.

Kolokotroni, M., & Giridharan, R. (2008). Urban heat island intensity in London: An investigation of the impact of physical characteristics on changes in outdoor air temperature during summer. *Solar Energy*, *82*(11), 986–998.
Kuhn, K., Campbell-Lendrum, D., & Davies, C. (2002). A continental risk map for malaria mosquito (Diptera: Culicidae) vectors in Europe. *Journal of Medical Entomology*, *39*(4), 621–630.
Kunst, A., Looman, C., & Mackenback, J. (1993). Outdoor air temperature and mortality in the Netherlands: A time-series analysis. *American Journal of Epidemiology*, *137*(3), 331–341.
Kutner, M., Nachtsheim, C., & Neter, J. (2004). *Applied linear regression models* (4th ed.). McGraw Hill.
Laaidi, K., Zeghnoun, A., Dousset, B., Bretin, P., Vandentorren, S., Giraudet, E., et al. (2012). The impact of heat islands on mortality in Paris during the August 2003 heat wave. *Environmental Health Perspectives*, *120*(2), 254–259.
Liaw, A., & Wiener, M. (2012). *Breiman and Cutler's random forests for classification and regression, R package.*
Liu, J. G., & Moore, J. M. (1998). Pixel block intensity modulation: Adding spatial detail to TM band 6 thermal imagery. *International Journal of Remote Sensing*, *19*, 2477–2491.
Maria, K., & Renganathan, G. (2008). Urban heat island intensity in London: An investigation of the impact of physical characteristics on changes in outdoor air temperature during summer. *Solar Energy*, *82*(11), 986–998.
Medina-Ramon, M., Zanobetti, A., Cavanagh, D., & Schwartz, J. (2006). Extreme temperatures and mortality: Assessing effect modification by personal characteristics and specific cause of death in a multi-city case-only analysis. *Environmental Health Perspectives*, *114*(9), 1131–1136.
Melgani, F., & Bruzzone, L. (2004). Classification of hyperspectral remote sensing images with support vector machines. *IEEE Transactions on Geoscience and Remote Sensing*, *42*(8), 1778–1790.
Meteotest (2010). Meteonorm handbook, Part III: Theory part 2. Accessed online in February 9 (2011). http://www.meteonorm.com/media/pdf/mn6_software.pdf
Meyer, D., Dimitriadou, E., Hornik, K., Weingessel, A., & Leisch, F. (2012). *Misc functions of the department of statistics (e1071), TU Wien, R package.*
Mostovoy, G. V., King, R. L., Reddy, K. R., Kakani, V. G., & Filippova, M. G. (2006). Statistical estimation of daily maximum and minimum air temperatures from MODIS LST data over the state of Mississippi. *GIScience and Remote Sensing*, *43*(1), 78–110.
Mountrakis, G., Im, J., & Ogole, C. (2011). Support vector machines in remote sensing: A review. *ISPRS Journal of Photogrammetry and Remote Sensing*, *66*(2011), 247–259.
Murray, K., & Conner, M. M. (2009). Methods to quantify variable importance: Implications for the analysis of noisy ecological data. *Ecology*, *90*, 348–355.
Nichol, J. E., Fung, W. Y., Lam, K. -S., & Wong, M. S. (2009). Urban heat island diagnosis using ASTER satellite images and 'in situ' air temperature. *Atmospheric Research*, 276–284.
Nichol, J. E., & To, P. H. (2012). Temporal characteristics of thermal satellite images for urban heat stress and heat island mapping. *ISPRS Journal of Photogrammetry and Remote Sensing*, *74*, 153–162.
Ocak, I., & Seker, S. (2013). Calculation of surface settlements caused by EPBM tunneling using artificial neural network, SVM, and Gaussian processes. *Environmental Earth Sciences*, http://dx.doi.org/10.1007/s12665-012-2214-x.
Oke, T. (1976). The distinction between canopy and boundary-layer urban heat islands. *Atmosphere*, *14*(4), 268–277.
Oke, T. (1988). The urban energy balance. *Progress in Physical Geography*, *12*, 471–508.
Oke, T., & Hay, J. (1994). *The climate of Vancouver* (2nd ed.). *B.C. Geographical Series*, *50*, Vancouver, British Columbia: Tantalus Press.
Oke, T. R., & Maxwell, G. B. (1975). Urban heat island dynamics in Montreal and Vancouver. *Atmospheric Environment*, *9*(2), 191–200.
Oommen, T., Misra, D., Twarakavi, N., Prakash, A., Sahoo, B., & Bandopadhyay, S. (2008). An objective analysis of support vector machine based classification for remote sensing. *Mathematical Geosciences*, *40*(4), 409–424.
Pal, M., & Mather, P.M. (2005). Support vector machines for classification in remote sensing. *International Journal of Remote Sensing*, *26*(5), 1007–1011.
Prihodko, L., & Goward, S. N. (1997). Estimation of air temperature from remotely sensed surface observations. *Remote Sensing of Environment*, *60*(3), 335–346.
R Core Development Team (2008). R: A language and environment for statistical computing. http://www.R-project.org/
Runnalls, K., & Oke, T. (2000). Dynamics and controls of the near-surface heat island of Vancouver, British Columbia. *Physical Geography*, *21*(4), 283–304.
Saaroni, H., & Baruch, Z. (2010). Estimating the urban heat island contribution to urban and rural air temperature differences over complex terrain: Application to an arid city. *Journal of Applied Meteorology and Climatology*, *49*, 2159–2166.
Sandholt, I., Rasmussen, K., & Andersen, J. (2002). A simple interpretation of the surface temperature/vegetation index space for assessment of surface moisture status. *Remote Sensing of Environment*, *79*(2–3), 213–224.
Sieber, R. (2006). Public participation geographic information systems: A literature review and framework. *Annals of the Association of American Geographers*, *96*(3), 491–507.
Singh, R., Joshi, P., & Kishtawal, C. (2006). A new method to determine near surface air temperature from satellite observations. *International Journal of Remote Sensing*, *27*(14), 2831–2846.
Statistics Canada (2007). *Greater Vancouver, British Columbia (Code5915) (table). 2006 Community Profiles*. 2006 Census. Statistics Canada Catalogue no. 92-591-XWE (Ottawa. Released March 13, 2007).
Stisen, S., Sandholt, I., Norgaard, A., Fensholt, R., & Eklundh, L. (2007). Estimation of diurnal air temperature using MSG SEVIRI data in West Africa. *Remote Sensing of Environment*, *110*(2), 262–274.
Strobl, C., Malley, J., & Tutz, G. (2009). An introduction to recursive partitioning: Rational, application, and characteristics of classification and regression trees, bagging, and random forests. *Psychological Methods*, *14*(4), 323–348.
Stumpf, A., & Kerle, N. (2011). Object-oriented mapping of landslides using random forests. *Remote Sensing of Environment*, *115*, 2564–2577.
Su, J., Brauer, M., & Buzzelli, M. (2008). Estimating urban morphometry at the neighborhood scale for improvement in modeling long-term average air pollution concentrations. *Atmospheric Environment*, *42*, 7884–7893.
Sun, D., Li, Y., & Wang, Q. (2009). A unified model for remotely estimating chlorophyll a in Lake Taihu, China, based on SVM and in situ hyperspectral data. *IEEE Transactions on Geoscience and Remote Sensing*, *47*(8), 2957–2965.
Sun, Y. J., Wang, J. F., Zhang, R. H., Gillies, R. R., Xue, Y., & Bo, Y. C. (2005). Air temperature retrieval from remote sensing data based on thermodynamics. *Theoretical and Applied Climatology*, *80*(1), 37–48.
Timm, B., & McGraigal, K. (2012). Fine-scale remotely-sensed cover mapping of coastal dune and salt marsh ecosystems at Cape Cod National Seashore using Random Forests. *Remote Sensing of Environment*, *127*, 106–117.
Tomlinson, C., Chapman, L., Thornes, J., & Baker, C. (2011). Including the urban heat island in spatial heat health risk assessment strategies: A case study for Birmingham, UK. *International Journal of Health Geographics*, *10*, 42.
Unger, J., Sümeghya, Z., & Zobokib, J. (2001). Temperature cross-section features in an urban area. *Atmospheric Research*, *58*(2), 117–127.
Vancutsem, C., Ceccato, P., Dinku, T., & Connor, S. J. (2010). Evaluation of MODIS land surface temperature data to estimate air temperature in different ecosystems over Africa. *Remote Sensing of Environment*, *114*(2), 449–465.
Vogt, J., Viau, A. A., & Paquet, F. (1997). Mapping regional air temperature fields using satellite derived surface skin temperatures. *International Journal of Climatology*, *17*, 1559–1579.
Weng, Q., Lu, D., & Schubring, J. (2004). Estimation of land surface temperature–vegetation abundance relationship for urban heat island studies. *Remote Sensing of Environment*, *89*, 467–483.
Willmott, C. J., & Matsuura, K. (2005). Advantages of the mean absolute error (MAE) over the root mean square error (RMSE) in assessing average model performance. *Climate Research*, *30*, 79–82.
Wong, M., Nichol, J., & Ng, E. (2011). A study of the "wall effect" caused by proliferation of high-rise buildings using GIS techniques. *Landscape and Urban Planning*, *102*, 245–253.
World Meteorological Organization (1996). *Guide to meteorological instruments and methods of observation* WMO-No. 8 (6th ed.) (Geneva).
Xu, Y., Qin, Z., & Shen, Y. (2012). Study on the estimation of nearsurface air temperature from MODIS data by statistical methods. *International Journal of Remote Sensing*, *33*(24), 7629–7643.
Zakšek, K., & Oštir, K. (2012). Downscaling land surface temperature for urban heat island diurnal cycle analysis. *Remote Sensing of Environment*, *117*, 114–124.
Zakšek, K., & Schroedter-Homscheidt, M. (2009). Parameterization of air temperature in high temporal and spatial resolution from a combination of the SEVIRI and MODIS instruments. *ISPRS Journal of Photogrammetry and Remote Sensing*, *64*(4), 414–421.
Zhu, W., Lu, A., & Jia, S. (2013). Estimation of daily maximum and minimum air temperature using MODIS land surface temperature products. *Remote Sensing of Environment*, *130*(2013), 62–73.